

# **The influence of drug solubility and sampling frequency on metformin and glibenclamide release from double-layered particles: experimental analysis and mathematical modelling**

T. Shams<sup>1,2</sup>, F. Brako<sup>2</sup>, S. Huo<sup>3</sup>, A. H. Harker<sup>3</sup>, U. Edirisinghe<sup>5</sup>, M. Edirisinghe<sup>1\*</sup>

<sup>1</sup>*Department of Mechanical Engineering, University College London, Torrington Place, London, WC1E 7JE, UK*

<sup>2</sup>*Department of Pharmaceutics, University College London School of Pharmacy, Brunswick Square, London, WC1N 1AX, UK*

<sup>3</sup>*London Centre for Nanotechnology, Kings Cross, London, WC1H 0AH, UK*

<sup>4</sup>*Department of Physics and Astronomy and London Centre for Nanotechnology, University College London, London, WC1E 6BT, UK*

<sup>5</sup>*Accident and Emergency Department, Hillingdon Hospital, Pield Heath Rd, Uxbridge, Middlesex UB8 3NN, UK*

## *Abstract*

Co-axial electrohydrodynamic atomization was used to prepare core/shell polymethylsilsesquioxane particles for co-delivery of metformin and glibenclamide in a sustained release manner. The drug-loaded microparticles were mostly spherical and uniformly distributed in size, with average diameters between 3 and 5µm across various batches. FTIR was used to confirm the presence of drugs within the particles while X-ray diffraction studies revealed drugs encapsulated existed predominantly in the amorphous state. Intended as systems that potentially can act as depot formulations for long term release of antidiabetics, a detailed analysis of drug release from these particles was necessary. Drugs of different solubilities were selected in order to study the effects of drug solubility from a core/shell particle system. Further analyses to determine how

conditions such as release into a limited volume of media, sampling rate and partitioning of drug between the core and shell layers influenced drug release were conducted by comparing experimental and mathematically modelled outcomes. It was found that while solubility of drug may affect release from such systems, rate of removal of drug (sampling) which upsets local equilibrium at the particle/solution interface prompting a rapid release to redress the equilibrium influenced release more.

### *1. Introduction*

The International Diabetes Federation estimated about 415 million adults as having diabetes as at 2015 and projected this figure to be 642 million by 2040. About 90% of these are classified under Type2 diabetes, a condition mainly driven by obesity, sedentary lifestyle and increased consumption of unhealthy diets including sugar-sweetened beverages [1, 2] . Oral administration of hypoglycaemic agents, often a biguanide, e.g. metformin, has predominantly been the first line option when medication is required for managing type 2 diabetes mellitus [3, 4]. In most patients with type 2 diabetes two defects coexist. This includes defective insulin sensitivity and defective insulin secretion. Both of these abnormalities contribute to hyperglycaemia [5] . Thus, oral therapy with either biguanides such as metformin that increase sensitivity of peripheral tissues to insulin, or sulfonylureas such as glibenclamide, which stimulate insulin secretion, are sensible approaches to type 2 diabetes mellitus [6] . Sulfonylureas are thought to act by binding to sulfonylurea receptor (SUR)-1 subunits of pancreatic beta potassium channels leading to their closure and subsequent membrane depolarization which open up voltage-dependent  $Ca^{2+}$  channels. This ensures a build-up of intracellular calcium concentrations, consequentially mediating the release of insulin [7] . Biguanides on the other hand work through complex physiological pathways mediated by both AMP-

activated protein kinase (AMPK)-dependent and AMPK-independent mechanisms to reduce hepatic glucose production [8] .

Each of them can be used solely or in combined form when either of them on their own is not sufficient on bringing down or maintaining blood sugar at safe levels. However, there remain issues of patient non-adherence which are generally driven by multiple daily dosing requirements [9, 10] . Reflecting on how effective these active pharmaceutical ingredients have been in oral formulations for the control of blood sugar levels, the potential of formulating these as depot preparations for long-term release is an appealing proposal. Micro and nanoparticle formulations of these antidiabetics to be injected as depot preparations seem an ideal approach as these structures have demonstrated a number of advantages including ease with which they are injected into tissues or intravenously [11] .

In this study, electrohydrodynamic (EHD) forming has been utilized in developing core-shell particle structures [12] where either glibenclamide (model sulfonylurea drug) or metformin (model biguanide drug) occupies the core while polymethylsilsesquioxane (PMSQ) polymer makes the shell surrounding the active ingredient [13, 14] . PMSQ was chosen as it offers chemical durability and being biocompatible, it is a desirable material for applications in biomedical engineering [15, 16] . In addition to being the most commonly used oral hypoglycaemic agents, the remarkable water solubility differences between metformin and glibenclamide are the reasons for selecting these as model drugs [17] , so that the influence of solubility on drug release from these particles can be studied [18, 19] . Various microscopic and spectroscopic techniques were employed in elucidating the physical characteristics and molecular composition of these structures. To determine the possibility of metformin and glibenclamide particles functioning as depot drug releasing systems, a more detailed view of release profiles as influenced by

particle composition, morphology and physical properties was developed. Furthermore, the likely effects of varying experimental procedures such as frequency of sampling which hitherto had been considered inconsequential to release outcomes were studied. Trends observed as well as mathematical modelling of experimental data derived from release data are discussed, offering further insights into the release of drug from a system essentially made of uniformly distributed bi-layered spherical particles.

## *2. Materials and Methods*

### *2.1 Materials*

Polymethylsilsesquioxane (PMSQ) with an average molecular weight  $7465 \text{ g mol}^{-1}$  was provided by Wacker Chemie AG, GmbH (Burghausen, Germany). Metformin hydrochloride with molecular weight of  $165.62 \text{ g mol}^{-1}$  was obtained from Sigma-Aldrich (Poole, UK). Glibenclamide used in this work was purchased from MP Biomedicals (Loughborough, UK). General purpose research grade ethanol (99% purity) was purchased from Sigma-Aldrich (Poole, UK). All of the above were used as received.

#### *2.2.1 Solutions for making particles*

A 15% (w/v) PMSQ solution was prepared by dissolving an appropriate amount of PMSQ in ethanol and stirred to ensure complete dissolution. To prepare the metformin particles (S1), 10 mg of the drug was dissolved in 80 ml of ethanol, and for glibenclamide particles (S2), 20 mg glibenclamide was dissolved in 80 ml ethanol. For the combined drug formulation (S3), 10 mg metformin and 20 mg glibenclamide were dissolved in 80 ml ethanol. Ethanol was used as both drugs, metformin and glibenclamide as well as PMSQ are freely soluble in it and rapidly evaporates during electrospraying.

Characteristics of the prepared solutions including electrical conductivity, surface tension and viscosity, measured at ambient conditions, are shown in Table 1. Electrical conductivity was determined using a conductivity probe, Jenway 3540 pH/conductivity meter (Cole-Palmer, Stone, UK).

*Table 1 Properties of solutions used in developing the particles*

| Solution  | Surface Tension<br>(mN/m) | Viscosity<br>(mPa s) | Electrical Conductivity<br>( $\mu$ S/m) |
|---|---------------------------|----------------------|---|
| Metformin HCL 10mg in 80ml<br>EtOH                      | 21.2 $\pm$ 0.3            | 0.92                 | 25.4 $\pm$ 0.3                          |
| Glibenclamide 20mg in 80 ml<br>EtOH                     | 21.4 $\pm$ 0.2            | 0.97                 | 32.3 $\pm$ 0.3                          |
| 10mg Metformin HCL + 20mg<br>Glibenclamide in 80ml EtOH | 21.5 $\pm$ 0.2            | 0.93                 | 23.2 $\pm$ 0.4                          |
| PMSQ 15% w/v in EtOH                                    | 21.8 $\pm$ 0.3            | 1.36                 | 0.66 $\pm$ 0.0                          |

Viscosity was measured using a U-tube viscometer 75 mL Cannon- Fenske Routine Viscometer (Cannon Instruments, Pennsylvania, USA), while a Kruss tensiometer Model-K9 (Kruss GmbH, Hamburg, Germany) was used to obtain surface tension values. Distilled water was used in order to calibrate the viscometer, tensiometer and electrical conductivity probe.

### *2.2.2 Preparation of the capsules*

The prepared solutions were carefully placed into 10 mL airtight syringes to avoid bubble formation during processing, and set to be driven by a pump, Harvard PHD 4400 (Harvard Apparatus, Edenbridge, UK) to deliver a precise volume per unit time. A co-axial needle system with inner diameters of 0.6 mm and 1.52 mm and outer diameters of 0.9

mm and 2.03 mm, were connected to a high precision voltage power supply. The positive electrode of a high precision DC voltage power supply HCP 35 65000 (Fug Elektronik, Rosenheim, Germany) was connected to the needle tip. The ground electrode was fixed onto a rectangular metal collector plate.

*Table 2 Experimental parameters for each polymeric system*

| Polymer System                                 | Inner Flow Rate ( $\mu\text{l}/\text{min}$ ) | Outer Flow Rate ( $\mu\text{l}/\text{min}$ ) | Applied Voltage (kV) |
|--|--|--|----------------------|
| S1: Metformin-loaded particles                 | 2  | 8  | 11                   |
| S2: Glibenclamide-loaded particles             | 6  | 18   | 12                   |
| S3: Metformin + Glibenclamide-loaded particles | 6  | 18   | 11                   |

Experiments were carried out under ambient conditions with average room temperature 21°C and relative humidity 40-60% throughout the studies. Electrical potential was applied across a fixed working distance of 150 mm between the tip of the co-axial needles and the grounded collection platform. The flow rates and the range of applied voltage were tuned in order to establish a stable cone-jet for each system. Different spherical structures incorporating single or two drugs in the core surrounded by outer polymeric layer were made subsequently. The optimal combinations of flow rates and applied voltage that enabled the processing of various batches of particles are shown in Table 2.

### *2.2.3 Particle morphology and size distribution*

Drug-loaded microparticles were examined by scanning electron microscopy (SEM). The particles were gold sputter-coated with a rotary pump coater Q150R ES (Quorum Technologies, Laughton, UK) for 3 min preceding SEM imaging by Hitachi S-3400n (Hitachi High Technologies, Tokyo, Japan). The size distributions of the particles were

obtained from SEM images using Image J software, where 300 particles from each batch were measured at random and the mean diameter was calculated. The size distribution curves were obtained by examining raw measurements using the Image J application (National Institutes of Health, Maryland, USA) and OriginPro software (OriginLab, Northampton, USA). The images and corresponding size distributions are shown in Figure 1.

#### *2.2.4 X-ray powder diffraction*

The particle structures and crystalline forms loaded active ingredients were studied using D/Max-BR diffractometer (RigaKu, Tokyo, Japan) with Cu K $\alpha$  radiation. Analyses were conducted at 40 mV and 30 mA over 2 $\theta$  range of 5–45° at a rate of 2°/min. Data obtained were converted to diffractograms and evaluated using OriginPro 7.0 software (OriginLab Corporation, Northampton, USA).

#### *2.2.5 Fourier transform infrared spectroscopy (FTIR)*

In order to establish if the particles produced contained active ingredients as intended, the chemical compositions of the particles were investigated using Attenuated Total Reflection Fourier Transform Infrared spectroscopy (ATR–FTIR) measurements (Bruker Vertex 90 spectrometer), and spectrographs were interpreted using OPUS Viewer version 6.5 software. Each sample had 64 scans at a resolution of 4 cm<sup>-1</sup>. Spectra of the particles were compared to those of the individual drugs and polymers to identify characteristic functional groups in the processed materials. The same parameters were used for background scans before each sample was analysed.

#### *2.2.6 Focused ion beam (FIB) microscope*

Cross sectional images of the particles were prepared using ZEISS NV40 FIB/SEM, a cross-beam of focused ion and field emission gun (FEG) electron beam. In the experiments, a Ga ion beam 30 kV, 150 and 300 pA were used to cut the sphere sample and 1.5 kV electron beam was used for imaging the cross section using SE2 detector or BSE detector to obtain good quality SEM images. Particles were gold sputtered for 120 s and mounted on metallic studs.

### *2.2.7 Drug release studies*

To measure the amount of drug released from drug-loaded microparticles, a setup in which 40mg of sample was enclosed in a fine metal mesh to ensure total immersion of particles and placed in a vessel of 40 ml capacity. Body temperature conditions and continuous agitation at 80 rpm were maintained throughout the release study using a benchtop incubated shaker (Sciquip, Newtown, UK). Samples of volume 2 ml were taken at various intervals from the vessel. 2 ml blank media was added after each sampling to maintain a constant volume.

Ultraviolet-visible (UV-Vis) spectroscopy (Jenway 6305 UV/Visible spectrophotometer, Bibby Scientific, Staffordshire, UK) operating at 231 nm was used to quantify amount of drug sampled during this study. The operating wavelength was obtained after a spectrum scan of 0.003 mg/mL standard metformin solution between 200 and 280 nm. To convert absorbance readings to drug concentrations, a calibration curve and equation were obtained by measuring absorbance of standard metformin solutions in concentrations between 0.0008 and 0.003 mg/mL, from which metformin content in microparticles were derived. The same procedure was taken for quantification of glibencalmide at detection wavelength of 300 nm.

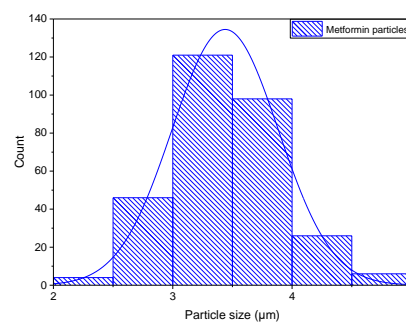
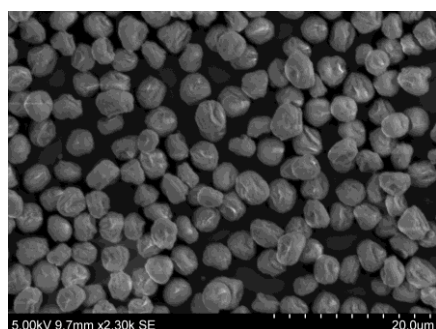
### 3 Results and discussions

#### 3.1 Particle size and size distribution

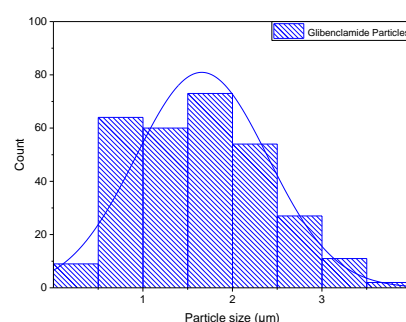
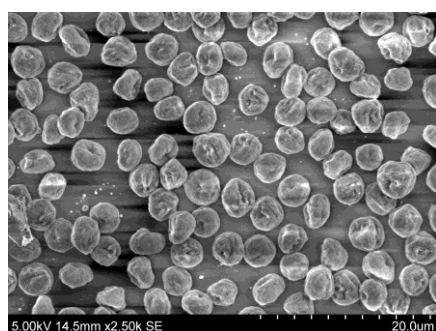
SEM images from the three batches were analysed for size and size distribution. The mean particle size (see Figure 1) was lowest for S2 at  $1.66 \pm 0.74 \mu\text{m}$ . This may be attributable to the highest electrical conductivity of the inner solution containing glibenclamide which aids EHD forming.

In comparison, for S3, with the same set flow rates, owing to a lower applied voltage and electrical conductivity of the inner solution, the average particle size is higher at  $4.79 \pm 0.48 \mu\text{m}$ .

**S1**



**S2**



S3

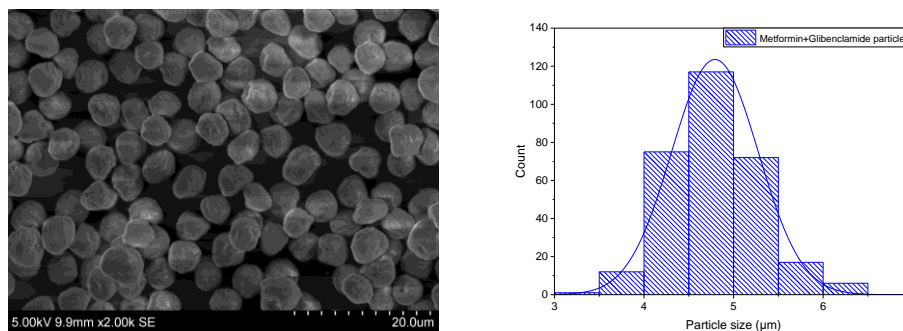


Figure 1 SEM images and the corresponding size distribution graphs of the developed drug delivery systems S1, S2 and S3. The smooth curve superimposed on each histogram represents a normal distribution with the same mean and standard deviation as the sample.

The same reason possibly explains the differences seen between S1 and S2. When compared, S2 contained an inner solution with lower electrical conductivity and hence required lower applied electrical potential. This resulted in a slight increase in the average particle size ( $3.44 \pm 0.44 \mu\text{m}$ ).

The differences in the set flow rates of S1 compared to that of S2 and S3 was due to formation of an unstable cone-jet that resulted in wide distribution size and inconsistency, therefore the selected values were chosen to ensure a narrow particle size distribution which is of immense importance in development of drug delivery system.

### 3.2 Structure and composition

The XRD patterns of the unprocessed PMSQ, metformin and glibenclamide as well as those of the prepared formulations are shown in Figure 2. The sharp diffraction peaks, representative of pure metformin were notable at  $2\theta$  angles of  $17^\circ$ ,  $22^\circ$ ,  $23^\circ$ ,  $25.27^\circ$  and  $45^\circ$ . This series of sharp and intense diffraction peaks are indicative of the crystalline state of pure metformin. The diffraction spectrum of pure glibenclamide also showed high peak intensities in the region of  $12^\circ$  to  $34^\circ$  of  $2\theta$ , indicating its crystalline state [20]. PMSQ showed the characteristic broad humps of an amorphous materials. As observed

in the diffractograms acquired for the developed formulation (S1 – S3), the amorphous nature was most prominent. In all formulations, no characteristic peaks of metformin and glibenclamide were detected. As revealed in the X-ray diffractograms of the drug-loaded formulations, the physical states of these particles are predominantly in amorphous state. The possibility of both drugs retaining some of their crystallinity following incorporation into the particles is also evident from the prominent peaks observed around  $11^\circ$ . Altogether, the diffractograms obtained for the particles can be interpreted to imply the drug-loaded structures existing as polymorphs.

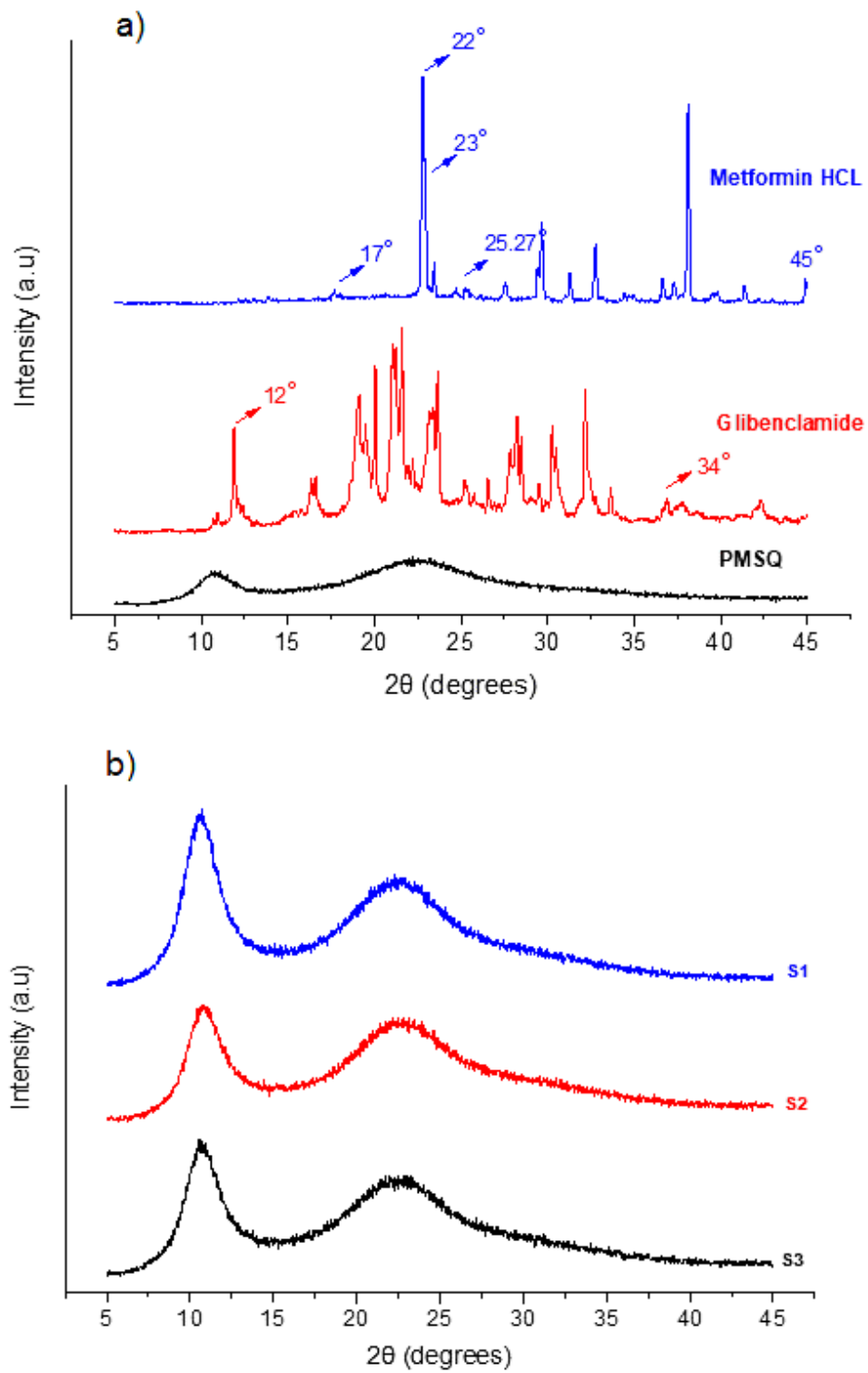


Figure 2 XRD spectrum of a) pure metformin HCL, glibenclamide and PMSQ and b) the developed formulations S1, S2 and S3.

### 3.3 Particle composition

The molecular compositions of the particles and possible interactions between drug and polymer during processing were investigated by FTIR. Spectra of the virgin materials and the particles produced are shown in Figure 3.

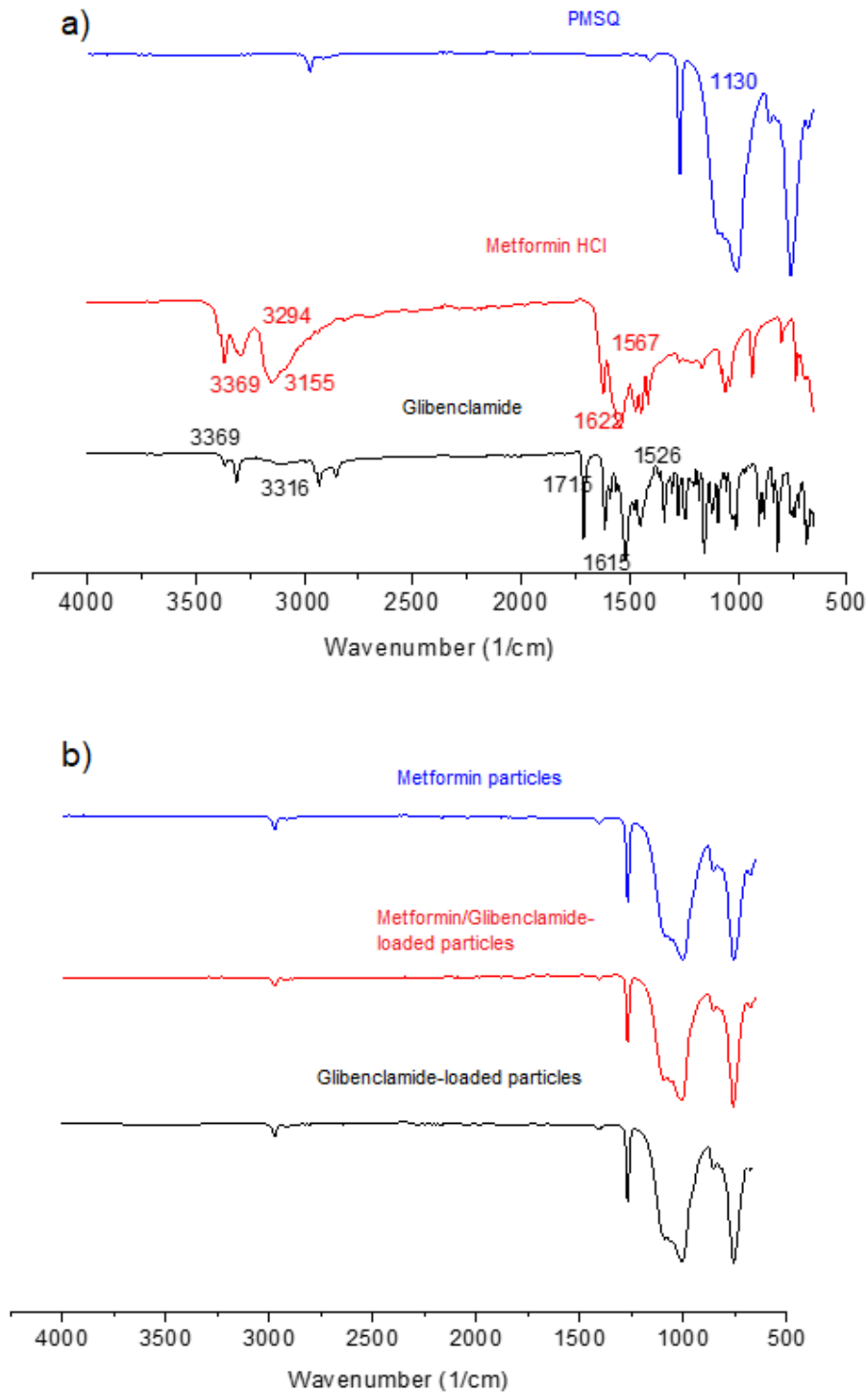


Figure 3 FTIR spectra of pure PMSQ, metformin HCL, glibenclamide and the developed formulations S1, S2 and S3.

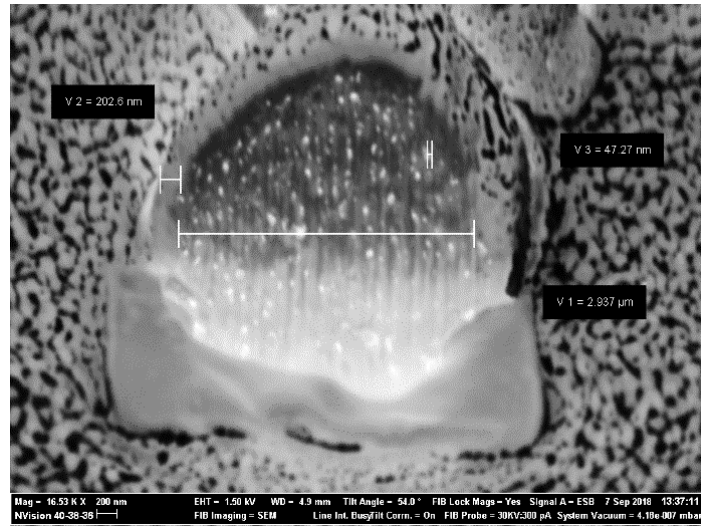
A characteristic band for PMSQ was observed at  $1130\text{ cm}^{-1}$  [16]. The spectrum of metformin showed characteristic bands at  $3369\text{ cm}^{-1}$  and  $3294\text{ cm}^{-1}$ , pointing to a primary amine (N-H) stretching vibration and a band at  $3155\text{ cm}^{-1}$  arising from secondary amine stretching. Characteristic bands at  $1622\text{ cm}^{-1}$  and  $1567\text{ cm}^{-1}$ , assigned to C-N stretching were also observed. The spectrum obtained for glibenclamide showed characteristic amide peaks at  $3369\text{ cm}^{-1}$ ,  $3316\text{ cm}^{-1}$  and  $1715\text{ cm}^{-1}$ . The urea carbonyl and N-H stretching vibrations were also observed at  $1615\text{ cm}^{-1}$  and  $1526\text{ cm}^{-1}$ , respectively. The absorption bands between  $2800\text{ cm}^{-1}$  and  $3200\text{ cm}^{-1}$  represent the aliphatic and aromatic C-H bond in this drug. The results obtained were in agreement with the published spectrum for the virgin drugs [21].

The FTIR spectra obtained for the developed formulations predominantly reflected peaks corresponding to PMSQ. This is to be expected as the formed particles were largely composed of PMSQ. Nonetheless, peaks at  $1567\text{ cm}^{-1}$ ,  $1622\text{ cm}^{-1}$  and  $1715\text{ cm}^{-1}$  though significantly diminished to reflect the quantities of drugs entrapped were also present, implying that indeed the particles contained drugs as intended.

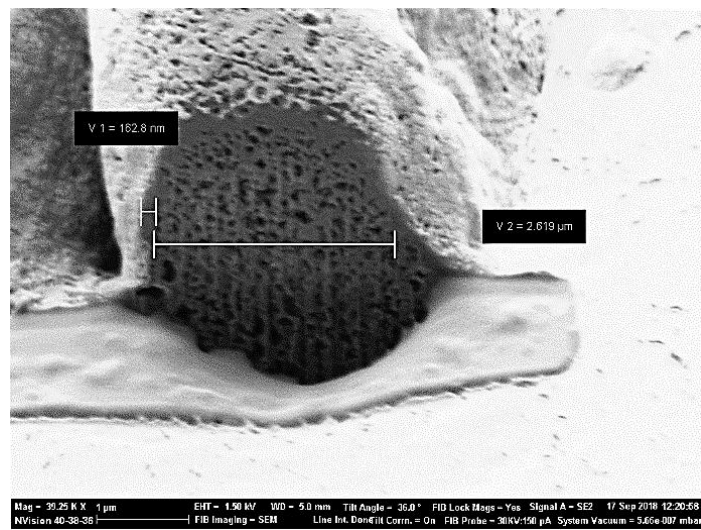
### *3.4 Particle morphology*

The morphology of the prepared formulations was studied using FIB/SEM (Fig. 4). The particles show a well-defined outer shell that encompasses a core when the majority of the respective encapsulated model drugs are enclosed in a capsule. The cross-sectional cuts through the particles are indicative of a porous core which can be explained by diffusion of the outer polymeric shell towards the centre of the particles as the solvent evaporation occurs. However, there is higher accumulation of polymer at the surface resulting in a solid surface and therefore the core/shell morphology evident in prepared formulations (S1, S2 and S3).

S1



S2



S3

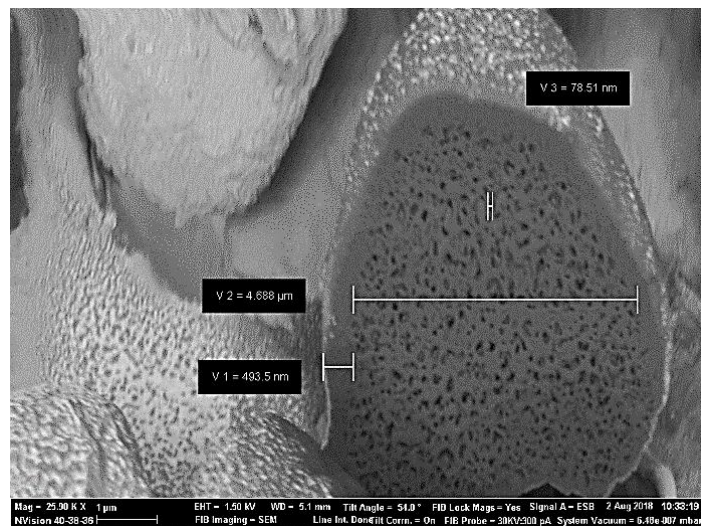


Figure 4 SEM/FIB cross-section images on cross section of the prepared formulations S1, S2 and S3 respectively after FIB cut.

### *3.5 Drug release*

A major part of this paper is dedicated to the release of antidiabetic drugs of different solubilities from polymeric nanoparticles through a combination of experimental data analysis and mathematical modelling.

#### *3.5.1 Influence of particle size and morphology*

The release profile of metformin was studied from formulations S1 and S3 for a duration of 12 hours and 168 hours respectively (Figure 5a). Burst release can be observed for the first 5 hours. This can be explained by diffusion of metformin towards the surface of the polymeric shell as solvent evaporation takes place. The slightly higher dissolution rate of the drug from S3 at 39% wt. can be due to the slightly larger particle size of  $4.79 \pm 0.48 \mu\text{m}$  that allows the incorporation of more unit surface bound drug per surface area. The burst release of metformin from S1 accounts for 26% wt. of the total drug content. Moreover, the flow rate ratio of metformin solution to PMSQ solution is higher for S3 at weight ratio 1:3 when compared to that of S1 at 1:4, this may also attribute to the slight discrepancies of metformin burst release from the developed formulations. A similar set of observations were made for glibenclamide (Figure 5b), the initial burst release was slightly higher from S3 when compared to S2. The EHD flow rates ratio was kept the same for both formulations. Therefore, the slightly higher dissolution rate of glibenclamide from S3 may be explained by more surface bound drug content in the particles produced. The burst release was also compared for that of glibenclamide and metformin from S3 to better understand the effect of aqueous drug solubility. As can be concluded from Figure 5c, metformin encountered notably higher dissolution rate which may be attributable to higher water solubility and hence relatively faster diffusion from the polymeric particles to the release medium. This effect is expected for highly water-soluble drugs. After the

first 5 hours of burst release, metformin and glibenclamide release from the combined S3 formulation nearly followed the same path (Figure 6a), resembling zeroth order release.

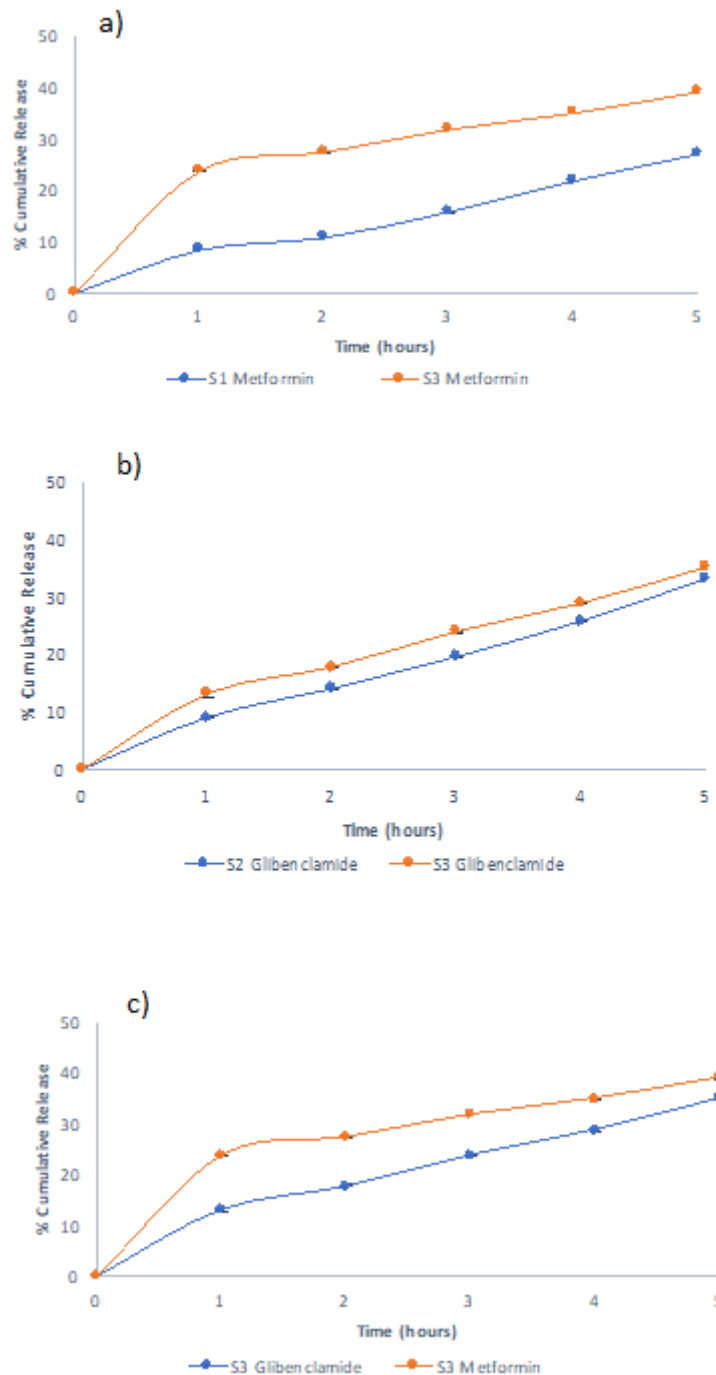


Figure 5: Cumulative drug release in the first 5 hours of a) metformin from S1 and S3 formulations b) glibenclamide from S2 and S3 formulations and c) cumulative release of glibenclamide and metformin percentage cumulative release from S3.

Due to the hydrophobic nature of the PMSQ polymeric carrier, the drug release is mainly driven by diffusion against the concentration gradient.

Whereby, higher drug content within the particles cause diffusion through the polymer chains in order to reach an equilibrium state. It is evident from the release profiles, that the frequency of sampling can also affect the dissolution rate, and this is considered in detail in section 3.5.2 below.

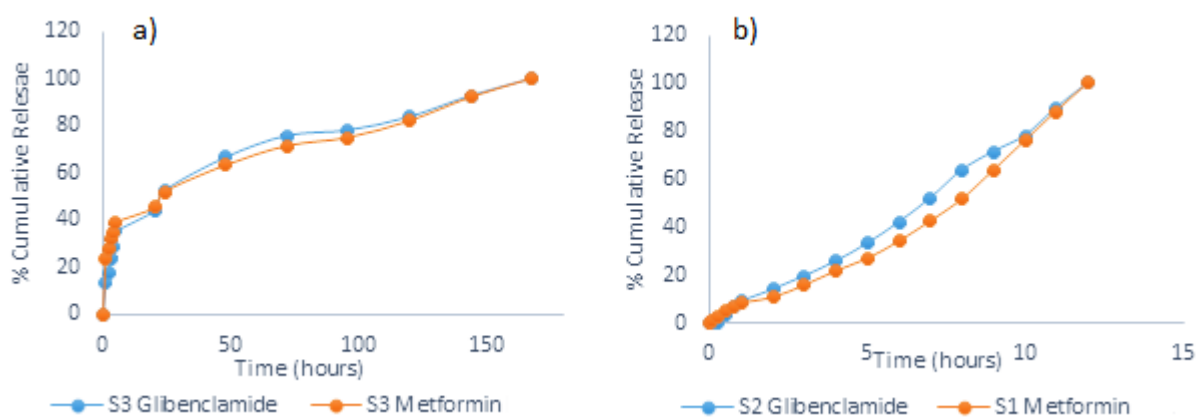


Figure 6 a) Glibenclamide and metformin cumulative release from S3 and b) glibenclamide and metformin cumulative release from S2 and S1.

Higher sampling frequency causes more disturbance to the system and results in further agitation of the drug delivery systems, this in turn also increases the dissolution rate as the release medium is continuously refreshed after aliquots are taken. The dissolution rate increases as there is a shorter time interval in between each sampling. An example of this can be seen in Figure 6a. For operational reasons samples were taken at 5, 20, 24 and 48 hours, and the effect of the short interval between 20 and 24 hours can be seen as a steep section of the release fraction. The same effect can be seen in Figure 7a and will be discussed in more detail in section 3.10 below. As shown in Figure 6b, the

glibenclamide release from S2 follows zeroth order release after the initial burst release for the first 5 hours, at which point the frequency of sampling is decreased and samples are withdrawn on hourly basis. The same was done for metformin HCL release studies from S1 formulation. Although glibenclamide is a poorly water-soluble drug, the dissolution rate is slightly higher when compared to metformin, which may be due to smaller average particle size of  $1.66 \pm 0.74 \mu\text{m}$ . This means there is higher surface area to volume ratio which results in a higher dissolution rate of the incorporated drug and is a characteristic of microparticles that are highly favourable for encapsulation of drugs with low aqueous solubility and therefore suffer from limited bioavailability. This is because there is a correlation between the dissolution rate and bioavailability of active ingredients. However, there is little difference between the release of metformin and glibenclamide that suggests the hydrophilic nature of the incorporated drug has little effect on the dissolution rate. This is in agreement with previous studies that have reported, that in general, electrospraying results in formation of microparticles that incorporate the active ingredient in their amorphous state, hence an accelerated drug release profile is observed [22] .

Nonetheless, it should be noted that there was higher initial amount of glibenclamide in the prepared formulations when compared to that of metformin, as adjusted due to the inherent solution properties in order to achieve a stable cone-jet in the EHD preparation of all formulations. As mentioned earlier, 10mg of metformin was used to make S1 formulation, 20 mg glibenclamide was used to prepare S2 formulation and for the combined drug formulation (S3), 10 mg metformin and 20 mg glibenclamide were used.

### *3.5.2 The effect of drug solubility vs sampling rate on drug release*

Theoretically, drug release from particles assume the so-called perfect sink conditions – that is, the concentration of the active ingredient in the medium outside the particles may be assumed to be negligible. The importance of maintaining appropriate conditions has been noted in the past [23] . It is relatively straightforward to describe this effect. If fluid were to be kept flowing past the particles, so that the particles were always surrounded by fluid containing no active ingredient, then eventually all of the active ingredient could be dissolved. In general, though, release rates are measured in a fixed volume of fluid, so the active ingredient may build up to a significant concentration. Suppose that the solubility of the active ingredient in the particle is much larger than in the surrounding fluid, so that in equilibrium the concentration in the particle  $C_p$  is related to that in the fluid  $C_f$ , then  $C_p = K_p C_f$  where  $K_p$  is the partition coefficient. In general, the volume of the particles  $V_p$  will be small compared to the volume of the fluid  $V_f$  so the ratio can be written as  $w = V_p/V_f$ . If the system with initial concentrations  $C_{p0}$  in the particles and 0 in the fluid is left until equilibrium is reached with concentrations  $C_{p\infty}$  in the particles and  $C_{f\infty}$  in the fluid, then the released fraction will be  $1/(K_p w + 1)$ . In an experiment though, fluid is sampled and replaced hence the active ingredient concentration in the fluid  $C_f$  is repeatedly reduced, and more material diffuses out of the particle to re-establish the partition equilibrium. It is therefore possible to approach arbitrarily close to complete release, but on a timescale that is determined by the sampling rate. A similar situation holds in a core-shell particle. If spherical symmetry is assumed, with a core of radius  $a$ , outer radius of particle  $b$ , and partition coefficients  $K_1$  between the core and the shell,  $K_2$  between the external fluid and the shell, then if the outer fluid is not replaced during the experiment the final released fraction will be:

$$K_1 / (K_1 + K_2 w \sigma^3 + K_1 K_2 w (1 - \sigma^3)),$$

where  $\sigma = a/b$ .

It was therefore assumed that drug release from uniformly dispersed microparticles, where periodic sampling disrupts the established equilibrium by removal of drug from the immediate surrounding of the particles, the frequency of sampling i.e. the rate of drug removal (upsetting the equilibrium) more than the solubility of drug will determine how soon complete release of drug occurs. This assumption is confirmed by plots of cumulative drug release versus time (shown in Figures 7a and b) where nearly as much drug was released in a 12-hour study with much frequent sampling (hourly) as in a 7-day study with less sampling frequency. This observation led to further interrogation of the influence of sampling frequency on drug release from microparticles.

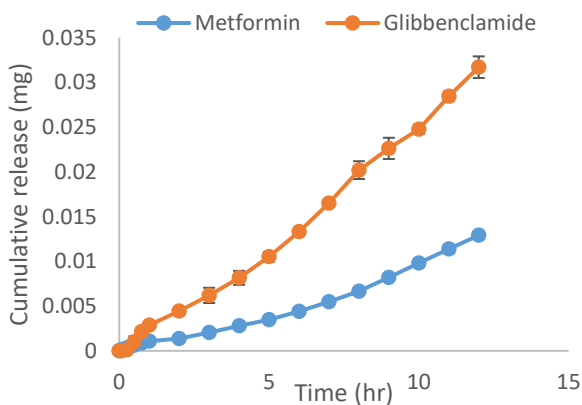
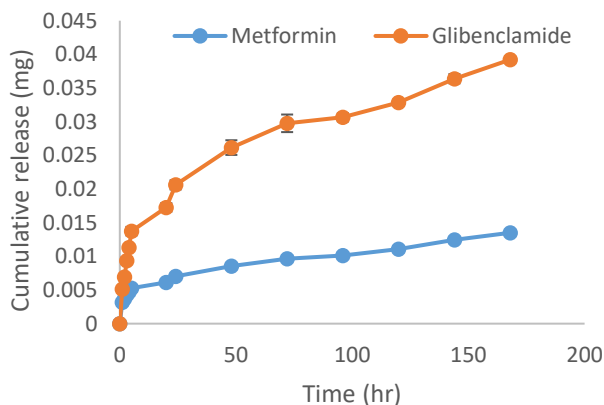


Figure 7: a) Cumulative release of metformine and glibenclamide from microparticles containing both drugs over 7 days and b) cumulative release of metformine and glibenclamide from microparticles containing both drugs over initial 12-hour period.

To better appreciate the theories used to explain the impact of sampling frequency on drug release from microparticles, a section showing how equations utilised were derived is given below.

### 3.6 Analytical theory

Consider particles in which an active ingredient is initially uniformly distributed in a porous core of radius  $a$ , and diffuses with diffusion coefficient  $D$  out of a spherical shell with outer radius  $b$ . It is convenient to work with a scaled time  $\tau = tD/b^2$ . Assume that the active ingredient is sufficiently mobile in the core for the concentration to be spatially uniform throughout the core. An approach similar to that of Paterson [24] can be used but as the geometry and the initial conditions for the present problem are different from Paterson's, the full theory is presented here. The key assumption is that the concentration in the shell,  $c_s$ , is controlled at its outer surface by the concentration in the fluid  $c_f$  and the partition coefficient  $K_2$ , and that a similar partition occurs between the core, in which the concentration is  $c_c$ , and the shell. Thus, the equations to be solved are:

$$\begin{aligned} \frac{\partial(rc_s(r,t))}{\partial t} &= D \frac{\partial^2(rc_s(r,t))}{\partial r^2} & (1) \\ c_c(0) &= c_0 & (2) \\ c_s(r,0) &= 0 & a \leq r \leq b \quad (3) \\ c_s(a,t) &= K_1 c_c(t) & t > 0 \quad (4) \\ c_s(b,t) &= K_2 c_f(t) & t > 0 \quad (5) \\ c_f(0) &= 0 & (6) \\ 4\pi a^2 \frac{\partial c_s(r,t)}{\partial r} \Big|_{r=a} &= \frac{4}{3}\pi a^3 \frac{dc_c(t)}{dt} & t > 0 \quad (7) \end{aligned}$$

$$-4\pi b^2 \frac{\partial c_p(r,t)}{\partial r} \Big|_{r=b} = V_f \frac{dc_f(t)}{dt} \quad t > 0. \quad (8)$$

It is convenient to transform to dimensionless form, defining

$$\begin{aligned} \frac{r}{b} &= \varrho \\ \frac{Dt}{b^2} &= \tau \\ \frac{rc_s(r,t)}{bc_0} &= u_s(r,t) \\ \frac{c_c(t)}{c_0} &= u_c(t) \\ \frac{c_f(t)}{c_0} &= u_f(t) \end{aligned}$$

with the volume ratio  $w$  and radius ratio  $\sigma$  previously defined to obtain

$$\frac{\partial(u_s(\varrho,\tau))}{\partial \tau} = \frac{\partial^2(u_s(\varrho,\tau))}{\partial \varrho^2} \quad (9)$$

$$u_c(0) = 1 \quad (10)$$

$$u_s(\varrho,0) = 0 \quad \sigma \leq \varrho \leq 1 \quad (11)$$

$$u_s(\sigma,\tau) = \sigma K_1 u_c(\tau) \quad \tau > 0 \quad (12)$$

$$u_s(1,\tau) = K_2 u_f(\tau) \quad \tau > 0 \quad (13)$$

$$u_f(0) = 0 \quad (14)$$

$$\frac{3}{\sigma \varrho} \left( \frac{\partial u_s(\varrho,\tau)}{\partial \varrho} - \frac{u_s(\varrho,\tau)}{\varrho} \right) \Big|_{\varrho=\sigma} = \frac{du_c(\tau)}{d\tau} \quad \tau > 0 \quad (15)$$

$$-\frac{3w}{\varrho} \left( \frac{\partial u_s(\varrho,\tau)}{\partial \varrho} - \frac{u_s(\varrho,\tau)}{\varrho} \right) \Big|_{\varrho=1} = \frac{du_f(\tau)}{d\tau} \quad \tau > 0. \quad (16)$$

Taking the Laplace transform, the equations involving derivatives become

$$p\tilde{u}_s(\varrho,p) = \frac{\partial^2(\tilde{u}_s(\varrho,p))}{\partial \varrho^2} \quad (17)$$

$$\frac{3}{\sigma \varrho} \left( \frac{\partial \tilde{u}_s(\varrho,p)}{\partial \varrho} - \frac{\tilde{u}_s(\varrho,p)}{\varrho} \right) \Big|_{\varrho=\sigma} = p\tilde{u}_c(p) - 1, \quad (18)$$

$$-\frac{3w}{\varrho} \left( \frac{\partial \tilde{u}_s(\varrho, p)}{\partial \varrho} - \frac{\tilde{u}_s(\varrho, p)}{\varrho} \right) \Big|_{\varrho=1} = p \tilde{u}_f(p). \quad (19)$$

It is convenient to write the transform variable in the form  $p = -s^2$ , whence we obtain from equation 17

$$\tilde{u}_p(\varrho, s) = -\frac{\varrho}{s^2} + A(s) \sin(s\varrho) + B(s) \cos(s\varrho).$$

Then, using the transformed interface conditions:

$$\tilde{u}_s(\sigma, p) = \sigma K_1 \tilde{u}_c(p) \quad (20)$$

$$\tilde{u}_s(1, p) = K_2 \tilde{u}_f(p) \quad (21)$$

together with equations (18) and (19), the coefficients  $A(s)$  and  $B(s)$  can be derived as:

$$A(s) = -K_1 \sigma^3 \left( (s^2 + 3K_2 w) \cos(s) + 3K_2 s w \sin(s) \right) / D(s) \quad (22)$$

$$B(s) = K_1 \sigma^3 \left( (s^2 + 3K_2 w) \sin(s) - 3K_2 s w \cos(s) \right) / D(s) \quad (23)$$

$$D(s) = 3s \left( 3K_1 K_2 w (\sigma - 1) + K_1 s^2 \sigma + K_2 s^2 w \sigma^2 \right) \cos(s(1 - \sigma)) \\ + \left( 9K_1 K_2 w - s^2 (s^2 + 3K_2 w) \sigma^2 + 3K_1 s^2 (1 + 3K_2 w s \sigma) \right) \sin(s(1 - \sigma)). \quad (24)$$

Inverting the Laplace transform by the usual contour integral method, we note that the expression has a simple pole at  $s = p = 0$  and pairs of poles at positive and negative values of  $s = s_n$  satisfying

$$D(s_n) = 0, \quad (25)$$

and evaluating the residues at the poles gives

$$u_s(\varrho, \tau) = \frac{K_1}{K_1 + K_2 w \sigma^3 + K_1 K_2 w (1 - \sigma^3)} + \sum_{n=1}^{\infty} \frac{A(s_n) \sin(s_n \varrho) + B(s_n) \cos(s_n \varrho)}{\Delta(s_n)} \exp(-s_n^2 \tau),$$

where the  $s_n$  are the roots of equation 25 and

$$2\Delta(s) = -s \left( K_1 \left( 3 + (6 + 9K_2 w) \sigma - 9K_2 w \sigma^2 \right) + \sigma^2 \left( s^2 (\sigma - 1) + 3K_2 w (2 + \sigma) \right) \right) \cos(s(1 - \sigma))$$

$$+ \left( \left( 6K_2 w + s^2 (4 - 3K_2 w (\sigma - 1)) \sigma^2 - 3K_1 (2 + s^2 (\sigma - 1) \sigma + 3K_2 w (1 + \sigma^2)) \right) \right) \sin(s(1 + \sigma)) \quad (26)$$

The fraction of the active ingredient released to the fluid may be evaluated simply by finding the shell concentration at  $\rho=1$  and the partition coefficient:

$$\varphi(t) = \frac{V_f c_f(t)}{V_c c_0} \quad (27)$$

$$\varphi(\tau) = \frac{u_s(1, \tau)}{w \sigma^3 K_2}. \quad (28)$$

Note that the shell-fluid partition coefficient and the volume ratio enter the resulting formulae only as the product  $K_2 w$ .

If the surrounding fluid is *continuously* sampled and refreshed, so that in a time interval  $d\tau$  a fraction  $f' d\tau$  is replaced the surface boundary condition becomes

$$-\frac{3}{b} V_p \frac{\partial c_s(r, t)}{\partial r} \Big|_{r=a} = V_f \frac{dc_f(t)}{dt} + f' c_f(t) \quad t > 0.$$

A similar Laplace transform technique may be used to solve the resulting equations, giving coefficients which we denote by  $A'$  and  $B'$

$$A'(s) = -K_1 \sigma^3 \left( (s^2 - f' + 3K_2 w) \cos(s) + 3K_2 s w \sin(s) \right) / D'(s) \quad (29)$$

$$B'(s) = K_1 \sigma^3 \left( (s^2 - f' + 3K_2 w) \sin(s) - 3K_2 s w \cos(s) \right) / D'(s) \quad (30)$$

$$D'(s) = 3s \left( 3K_1 K_2 w (\sigma - 1) + K_1 (s^2 - f') \sigma + K_2 s^2 w \sigma^2 \right) \cos(s(1 - \sigma)) + \left( 9K_1 K_2 s^2 w \sigma - s^2 (s^2 - f' + 3K_2 w) \sigma^2 - 3K_1 (s^2 - f' - 3K_2 w) \right) \sin(s(1 - \sigma)). \quad (31)$$

where the solutions of  $D'(s)=0$  must now be inserted into the expression for the concentration in the shell

$$u_s(\varrho, \tau) = \sum_{n=1}^{\infty} \frac{A'(s_n)\sin(s_n\varrho) + B'(s_n)\cos(s_n\varrho)}{\Delta'(s_n)} \exp(-s_n^2\tau),$$

where

$$\begin{aligned} 2s\Delta'(s) = & ((f'(3K_1 + s^2(-1+\sigma)\sigma^2) - s^2(K_1(3+(6+9K_2w)\sigma - 9K_2w\sigma^2) \\ & + \sigma^2(s^2(-1+\sigma) + 3K_2w(2+\sigma))))\cos(s(1-\sigma)) \\ & - s((2f' - 6K_2w + s^2(-4+3K_2w(-1+\sigma)))\sigma^2 + 3K_1(2 - s^2\sigma - f'(-1+\sigma)\sigma \\ & + s^2\sigma^2 + 3K_2w(1+\sigma^2)))\sin(s(1-\sigma)). \end{aligned}$$

As the solution outside is being continually refreshed the released fraction cannot be evaluated just using the concentration at the outer shell surface and the partition coefficient: instead we must compute the amount inside the core from  $K_1$  and  $u_s(\sigma, \tau)$ , the amount in the shell by integrating throughout the shell, and subtracting the result from the initial amount present. The expressions are simple to derive from equation (1), and:

$$\begin{aligned} \varphi'(\tau) = & 1 - \sum_n \left[ \frac{A'(s_n)}{s_n} \frac{3}{2} (\sin(s_n) - \sin(s_n\sigma) - s_n \cos(s_n) + s_n \sigma \cos(s_n\sigma)) \right. \\ & + \frac{B'(s_n)}{s_n} \frac{3}{2} (\cos(s_n) - \cos(s_n\sigma) - s_n \sin(s_n) - s_n \sigma \sin(s_n\sigma)) \\ & \left. + \frac{1}{K_1\sigma} (A'(s_n)\sin(s_n\sigma) + B'(s_n)\cos(s_n\sigma)) \right] \exp(-s_n^2\tau) / \Delta'(s_n). \end{aligned} \quad (32)$$

It is rather inconvenient to adapt this analytical result to the situation in which the fluid is periodically sampled and diluted, so we have adopted a numerical approach to treat

this. The Euler method, in which we define the concentrations in the particle on a regularly-spaced radial grid and take uniform time-steps, is a better way of resolving this, hence we write

$$c_p(i\Delta q, n\Delta\tau) = c_{i,n}, \quad 0 \leq i \leq N$$

with

$$c_{i,n+1} = c_{i,n} + \Delta\tau \frac{dc_{i,n}}{d\tau},$$

where we use the same dimensionless radius  $q$  and time  $\tau$  as before. We use a second-order finite difference approximation to the spatial derivatives (see, for example, Section 8.7 of Crank's monograph [Crank, 1956][25] to give

$$\frac{dc_{i,n}}{d\tau} = \begin{cases} \frac{6(c_{1;n} - c_{0;n})}{\Delta q^2}, & \text{for } i=0 \\ K_p c_{f;n}, & \text{for } i=M \\ \frac{(i+2)c_{i+1;n} - 2ic_{i;n} + (i-2)c_{i-1;n}}{2i\Delta q^2} + \frac{c_{i+1;n} - 2c_{i;n} + c_{i-1;n}}{2\Delta q^2}; & \text{otherwise.} \end{cases}$$

We have coded these expressions in *Mathematica*. In evaluating  $c_f$  we have numerically integrated the flux  $J = D \partial c_s(r,t) / \partial r$  over the particle surface to adjust the amount in solution. We allow samples of a fraction  $f$  of the solution to be extracted at regular intervals and replaced with fluid free of active ingredient, resulting in an instantaneous reduction in  $c_f$  by a factor  $(1-f)$ . We have found that 40 radial divisions give adequate accuracy; the time-step  $\Delta\tau$  is chosen to ensure numerical stability of the forward Euler scheme.

Having set the context within which to consider in detail, aspects of drug release from uniformly dispersed particles and particularly the influence of sampling frequency on drug release, we present a modelling defining sustained release of drug from particles under various conditions as described below:

### 3.7 Sustained Release into Limited Volume

Here we investigate the effects of release into a limited volume using the results of section 3.6. In these studies, we use a radius ratio  $\sigma=a/b=0.8$  and a core-shell partition coefficient  $K_1=1$  throughout. First, we confirm that in the limiting case of slow sampling the results approaches the unsampled case: this constitutes a check on the mathematical derivation. Figure 8a shows that the expected result is obtained.

We now consider the effect of varying  $K_2w$  on the release fraction. Figure 8b shows the dominant effect: the release fraction is limited, at large times, to  $1/(1+K_p w)$ .

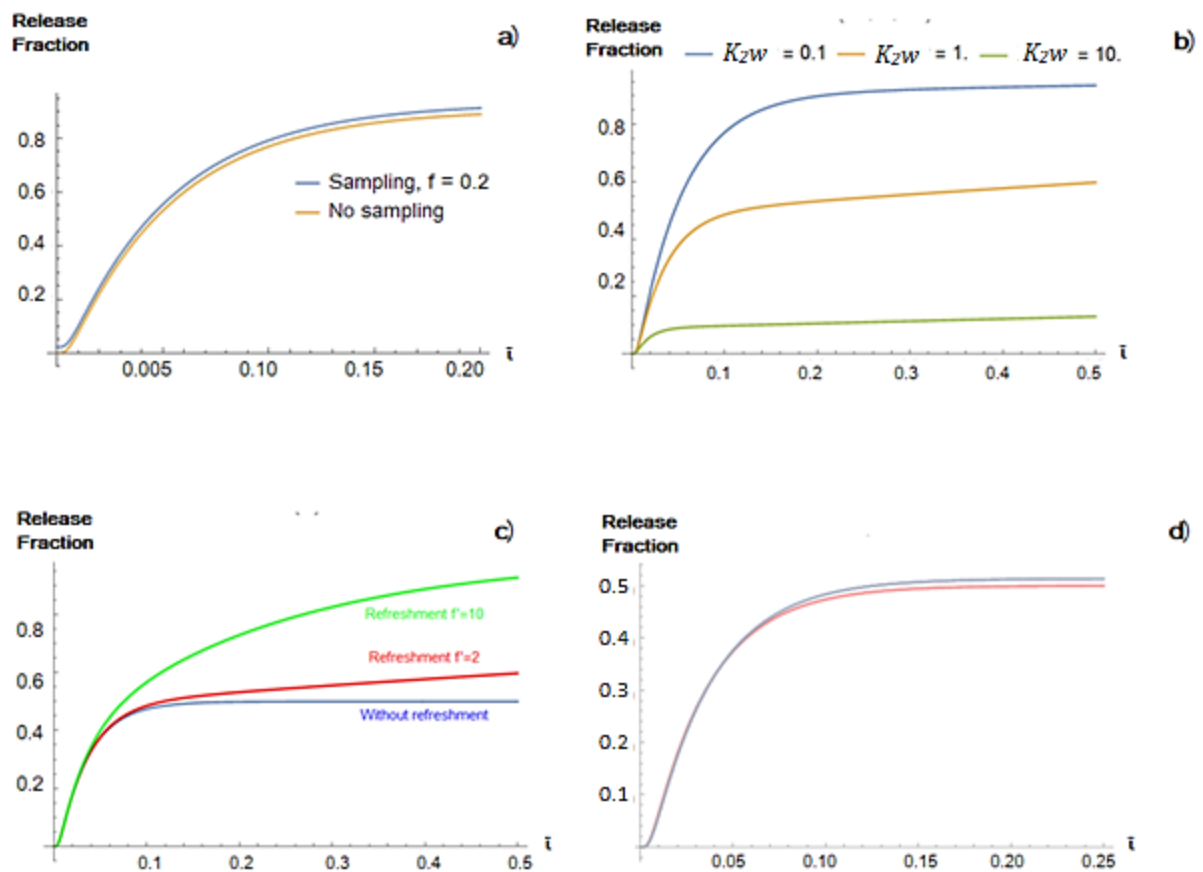


Figure 8: a): Confirmation that as  $\bar{t}$  becomes small as the release rate approaches the result for unsampled: the graphs compare the results from equation 28 with equation 32 with  $f'=0.2$ : with  $f'=0.1$  the graphs are indistinguishable, b) dependence of release fraction of active ingredient on finite volume conditions: the graph shows the result from equation 28 for various values of  $K_2w$ , c) comparison of the release into a finite volume with  $K_2w=1$  without (blue) or with (green) refreshment of the surrounding medium: these are computed with equation 28 and with equation 32 with  $f'=2$

and  $f' = 10$  and d) A comparison of the analytical result from equation 28 (red) with the release predicted by the finite difference method (blue) for the case  $K_2w = 1$ .

### *3.8 Sustained Release into Limited Volume with Continuous Sampling*

When  $f'$  is large, that is, when the time-scale for refreshing the surrounding fluid is short compared with the time-scale for diffusion in the particle ( $a^2/D$ ), an approximately linear release is observed when, without refreshment, the release would saturate. This is shown in Figure 8c. A near-linear release regime may be seen for appropriate combinations of parameters: it would be easy to mistake this for the linear release profile expected for diffusive release from a core-shell structure with perfect sink boundary conditions. It is also noteworthy that when the refresh rate is large the resulting release profile resembles closely the release with perfect sink boundary conditions. This is expected, but it does point to a possible difficulty in interpreting release rates measured in the laboratory.

### *3.9 Accuracy Check of Numerical Method*

Before using the finite difference model to investigate sampling effects, it is important to check that it is accurate. To confirm this, we show in Figure 8d a comparison of the analytical result from equation 28 (red) with the release predicted by the finite difference method (blue) for the case  $K_pw = 1$ . The agreement is satisfactory.

### *3.10 Release Rate with Sampling*

To exemplify the observations, we show in Figure 9a the release rate based on the finite difference results at a set of sampling times, specifically  $\tau = (0.01, 0.02, 0.03, 0.04, 0.05, 0.1, 0.2, 0.4, 0.6, 0.8, 0.9, 1.1, 1.3, 1.5, 1.7, 1.9, 2.1, 2.3, 2.5)$ . These are selected to form a sequence which is a scaled form of the sampling intervals used in the experiments reported in Section 3.5.1.

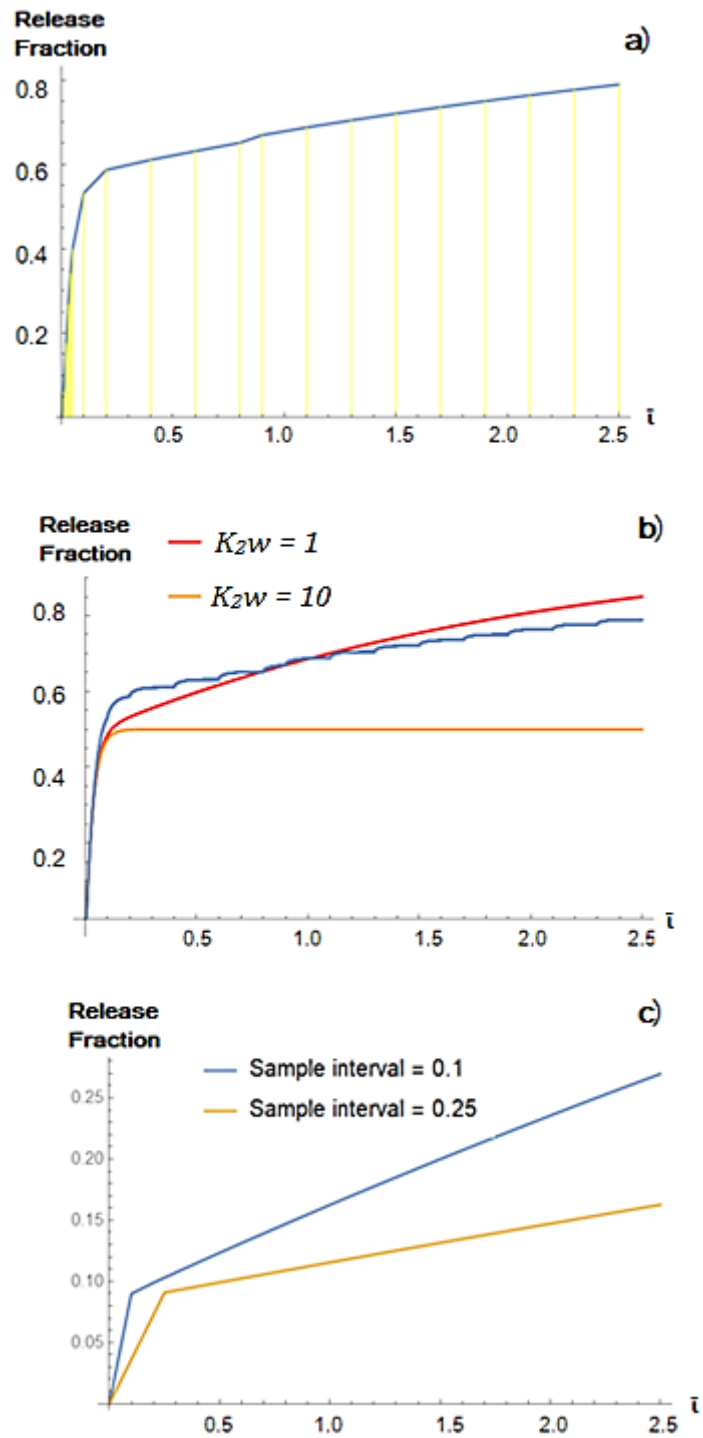


Figure9: a) Finite difference predictions of the release fraction obtained with sampling for the case  $K_2w = 10$  and sample fraction  $f=0.1$ . The yellow vertical lines show the sampling times, b) finite difference predictions of the release fraction obtained with sampling for the case  $K_2w=10$  and sample fraction  $f=0.1$ . The blue line shows the evolution of the release, following every step  $\Delta\tau$  of the calculation. The red line shows the release profile that would be obtained with constant sampling at a rate  $f' = 1$ , according to equation 32, and the orange line shows what would be seen without sampling and c) finite difference predictions of the release fraction obtained with different sampling for the case  $K_2w = 10$  and sample fraction  $f=0.1$

The control parameter was  $K_p w = 10$ , and the fraction of fluid withdrawn for sampling at each point was  $f=0.1$ . The yellow vertical lines on the graph show the sampling times. One notable feature is that when one shorter sampling interval is introduced (between  $\tau=0.8$  and  $\tau=0.9$ ) there is a visible kink in the release graph: this is also observable in the experimental results in Figures 6 and 7. Rather more insight can be gained by plotting the release at every time-step, rather than just at the sampling times. This is done in the blue line in Figure 9b, where the release expected predicted for sampling at a steady rate, equation 32, is shown in red and the result without sampling, equation 28, is shown in orange.

Two points are immediately obvious. First, sampling has had a marked effect on the total release (Figure 9c). Second, within each sample period it is clear that the reduction in solution concentration upsets the local equilibrium at the particle/solution interface, prompting a rapid release to redress the equilibrium, followed by slower release at the rate expected for the current concentration. If uniformly-spaced samples are taken, the resulting release profiles will be smooth, but the results will depend on the sampling interval. This is shown in Figure 9, where the release fractions are shown for the case  $K_2 w=1$ ,  $f=0.1$ , but with sampling intervals  $\Delta\tau=0.10$  and  $\Delta\tau=0.25$ . We should note that if the sampling interval is decreased so as to follow the earlier part of the release this will itself affect the release rate.

#### 4 Clinical Perspectives

In terms of the clinical context of this work, it has the potential to provide a novel and much needed solution to many clinical conundrums. Namely; patient drug compliance, high dosage associated side-effects, poor oral absorption, erratic glycaemic control and

therefore a reduction in the morbidity and mortality of diabetes - a common condition that has a rising incidence.

Diabetes is a global pandemic affecting 422 million worldwide - quadruple the number since 1980. The cost of diabetes to the NHS is over £1.5m an hour, this equates to over £25,000 being spent on diabetes every minute and an annual estimated spend of £14 billion pounds, with the cost of treating complications representing a much higher cost. It has micro and macrovascular complications that can have a devastating impact on patient quality of life, ranging from impotence to fulminant renal failure requiring dialysis, blindness and limb amputation in the extreme. The key to its successful treatment is therefore aggressive and tight control of blood sugar and prevention of ongoing hyperglycaemia in the tissues. The combined use of metformin and glibenclamide as in this study provides a multifaceted approach to this, by not only mediating insulin release but also boosting tissue sensitivity to insulin at the same time. Poor compliance to medication is a huge barrier to effective treatment of diabetes and has long been researched and acknowledged. This problem is complex and thought to be caused by patient perceived treatment efficacy, medication beliefs, cost of treatment, treatment complexity and convenience, as well as hypoglycaemia and other unwanted side effects such as diarrhoea. Diabetes can often be asymptomatic in the initial stages also affecting attitudes to treatment and medication use. This study could help to combat many of these aspects by reducing the number of drugs and the number of doses needed per day, as well as minimising the side effect profiles. This research also tackles the problem of bioavailability. For example, metformin has an absolute oral bioavailability of 40 to 60%, the drug loaded microparticles designed in this paper would significantly elevate this percentage and boost drug delivery. The promise of future combined drug

treatments in the depot microparticle form as routine and mass market prescription for diabetes is an exciting one and further research is needed to facilitate this vision.

## 5 Conclusions

In this study, we successfully formed, using electrohydrodynamics, a core/shell microparticle systems where an active drug, metformin, glibenclamide or a co-formulation of both drugs, occupied the core of the microparticles while the shell was entirely made of the polymer polymethylsilsesquioxane. While the individual particle sizes was influenced more by the electrical conductivity of the inner solution i.e. the portion forming the core of the particles, particle sphericity and size uniformity within a batch were to a large extent dependent on the flow rate. During formation therefore, flow rates were fine-tuned for the best possible shape of particles and uniformly distributed particles. In terms of molecular composition, FTIR confirmed groups seen in starting materials to be present particles, thus establishing that products indeed contained active drugs as was intended during formation. Furthermore, an XRD scan between 5° and 45° (2θ degrees) confirmed the drugs encapsulated within the microparticles existed predominantly in the amorphous state.

At the initial phase of drug release, it was observed that a higher amount of the more soluble metformin was released compared to the less soluble glibenclamide. This was expected and largely attributed to the higher water solubility of metformin driving up diffusion from the microparticle into the dissolution media. Significant initial bursts seen in all particles were analysed and are most likely caused by drug diffusing through the shell into the particle surface through solvent evaporation during particle formation.

A mathematical model of the system has been developed, based on the key parameters at play such as the core/shell structure, extent of partitioning of drugs between these two

layers, dissolution volume and its rate of refreshment. This has allowed a more detailed understanding of how drugs could be released from a two-layered system. The frequency of sampling is shown to upset the equilibrium at the interface between the particle and the release medium; the additional release required to reset this equilibrium has been shown to significantly influence the overall amount of drug released.

## References

- [1] Yoshida, Y. & Simoes, E.J. 2018 Sugar-Sweetened Beverage, Obesity, and Type 2 Diabetes in Children and Adolescents: Policies, Taxation, and Programs. *Current diabetes reports* **18**, 1-10.
- [2] Zheng, Y., Ley, S.H. & Hu, F.B. 2017 Global aetiology and epidemiology of type 2 diabetes mellitus and its complications. *Nat. Rev. Endocrinol.* **14**, 88-98 .
- [3] Chaudhury, A., Duvoor, C., Dendi, R., Sena, V., Kraleti, S., Chada, A., Ravilla, R., Marco, A., Shekhawat, N.S. & Montales, M.T. 2017 Clinical review of antidiabetic drugs: Implications for type 2 diabetes mellitus management. *Front. Endocrinol. (Lausanne)* **8**, 1-12.
- [4] Cheng, A.Y. & Fantus, I.G. 2005 Oral antihyperglycemic therapy for type 2 diabetes mellitus. *Can. Med. Assoc. J.* **172**, 213-226.
- [5] DeFronzo, R. 1992 Pathogenesis of type 2 (non-insulin dependent) diabetes mellitus: a balanced overview. *Diabetologia* **35**, 389-397.
- [6] Tosi, F., Muggeo, M., Brun, E., Spiazzi, G., Perobelli, L., Zanolin, E., Gori, M., Coppini, A. & Moghetti, P. 2003 Combination treatment with metformin and glibenclamide versus single-drug therapies in type 2 diabetes mellitus: a randomized, double-blind, comparative study. *Metabolism* **52**, 862-867.
- [7] Aittoniemi, J., Fotinou, C., Craig, T.J., de Wet, H., Proks, P. & Ashcroft, F.M. 2009 SUR1: a unique ATP-binding cassette protein that functions as an ion channel regulator. *Philos. Trans. R. Soc., B* **364**, 257-267.
- [8] Rena, G., Hardie, D.G. & Pearson, E.R. 2017 The mechanisms of action of metformin. *Diabetologia* **60**, 1577-1585.
- [9] Cramer, J.A. 2004 A systematic review of adherence with medications for diabetes. *Diabetes Care* **27**, 1218-1224.
- [10] Desai, D., Wang, J., Wen, H., Li, X. & Timmins, P. 2013 Formulation design, challenges, and development considerations for fixed dose combination (FDC) of oral solid dosage forms. *Pharm. Dev. Technol.* **18**, 1265-1276.
- [11] Kohane, D.S. 2007 Microparticles and nanoparticles for drug delivery. *Biotechnol. Bioeng.* **96**, 203-209.
- [12] Bock, N., Dargaville, T.R. & Woodruff, M.A. 2012 Electrospraying of polymers with therapeutic molecules: state of the art. *Prog. Polym. Sci.* **37**, 1510-1551.
- [13] Orlu-Gul, M., Topcu, A.A., Shams, T., Mahalingam, S. & Edirisinghe, M. 2014 Novel encapsulation systems and processes for overcoming the challenges of polypharmacy. *Curr. Opin. Pharmacol.* **18**, 28-34.

- [14] Mehta, P., Haj-Ahmad, R., Rasekh, M., Arshad, M.S., Smith, A., van der Merwe, S.M., Li, X., Chang, M.-W. & Ahmad, Z. 2017 Pharmaceutical and biomaterial engineering via electrohydrodynamic atomization technologies. *Drug Discovery Today* **22**, 157-165.
- [15] Nangrejo, M., Ahmad, Z., Stride, E., Edirisinghe, M. & Colombo, P. 2008 Preparation of polymeric and ceramic porous capsules by a novel electrohydrodynamic process. *Pharm. Dev. Technol.* **13**, 425-432.
- [16] Chang, M.-W., Stride, E. & Edirisinghe, M. 2010 Controlling the thickness of hollow polymeric microspheres prepared by electrohydrodynamic atomization. *J. R. Soc., Interface* **7**, S451-S460.
- [17] Cetin, M. & Sahin, S. 2016 Microparticulate and nanoparticulate drug delivery systems for metformin hydrochloride. *Drug delivery* **23**, 2796-2805.
- [18] Singh, A., Worku, Z.A. & Van den Mooter, G. 2011 Oral formulation strategies to improve solubility of poorly water-soluble drugs. *Expert Opin. Drug Delivery* **8**, 1361-1378.
- [19] Savjani, K.T., Gajjar, A.K. & Savjani, J.K. 2012 Drug solubility: importance and enhancement techniques. *ISRN Pharm.* **2012**, 1-10
- [20] Elbahwy, I.A., Ibrahim, H.M., Ismael, H.R. & Kasem, A.A. 2017 Enhancing bioavailability and controlling the release of glibenclamide from optimized solid lipid nanoparticles. *J. Drug Delivery Sci. Technol.* **38**, 78-89.
- [21] Essa, E.A., Elkotb, F.E., Eldin, E.E.Z. & El Maghraby, G.M. 2015 Development and evaluation of glibenclamide floating tablet with optimum release. *J. Drug Delivery Sci. Technol.* **27**, 28-36.
- [22] Shams, T., Parhizkar, M., Illangakoon, U., Orlu, M. & Edirisinghe, M. 2017 Core/shell microencapsulation of indomethacin/paracetamol by co-axial electrohydrodynamic atomization. *Mater. Des.* **136**, 204-213.
- [23] Gibaldi, M. & Feldman, S. 1967 Establishment of sink conditions in dissolution rate determinations. Theoretical considerations and application to nondisintegrating dosage forms. *J. Pharm. Sci.* **56**, 1238-1242.
- [24] Paterson, S. 1947 The heating or cooling of a solid sphere in a well-stirred fluid. *Proc. Phys. Soc.* **59**, 50-58.
- [25] Crank, J. 1956 *The Mathematics of Diffusion*. London, Oxford University Press.